



HAL
open science

New Late Neolithic (c. 7000–5000 BC) archeointensity data from Syria. Reconstructing 9000years of archeomagnetic field intensity variations in the Middle East

Yves Gallet, Miquel Molist Montaña, Agnès Genevey, Xavier Clop Garcia, Erwan Thébault, Anna Gómez Bach, Maxime Le Goff, Béatrice Robert, Inga Nachasova

► To cite this version:

Yves Gallet, Miquel Molist Montaña, Agnès Genevey, Xavier Clop Garcia, Erwan Thébault, et al.. New Late Neolithic (c. 7000–5000 BC) archeointensity data from Syria. Reconstructing 9000years of archeomagnetic field intensity variations in the Middle East. *Physics of the Earth and Planetary Interiors*, 2015, 238, pp.89-103. 10.1016/j.pepi.2014.11.003 . hal-01096917

HAL Id: hal-01096917

<https://hal.sorbonne-universite.fr/hal-01096917v1>

Submitted on 18 Dec 2014

HAL is a multi-disciplinary open access archive for the deposit and dissemination of scientific research documents, whether they are published or not. The documents may come from teaching and research institutions in France or abroad, or from public or private research centers.

L'archive ouverte pluridisciplinaire **HAL**, est destinée au dépôt et à la diffusion de documents scientifiques de niveau recherche, publiés ou non, émanant des établissements d'enseignement et de recherche français ou étrangers, des laboratoires publics ou privés.

1 **New Late Neolithic (c.7000-5000 BC) archeointensity data from Syria.**
2 **Reconstructing 9000 years of archeomagnetic field intensity variations in the**
3 **Middle East**

4 Yves Gallet ^a, Miquel Molist Montaña ^b, Agnès Genevey ^c, Xavier Clop García ^b, Erwan
5 Thébault ^{a,d}, Anna Gómez Bach ^b, Maxime Le Goff ^a, Béatrice Robert ^e, Inga Nachasova ^f

6 ^a *Institut de Physique du Globe de Paris, Sorbonne Paris Cité, Université Paris Diderot, UMR*
7 *7154 CNRS, F-75005 Paris, France*

8 ^b *SGR SAPPO. Prehistory Department, Facultat de Filosofia i Lletres, Edifici B, Universitat*
9 *Autònoma de Barcelona 08193 Bellaterra, Barcelona, Spain*

10 ^c *UPMC Université Paris 06, UMR CNRS 8220, Laboratoire d'Archéologie Moléculaire et*
11 *Structurale, LAMS, F-75005 Paris, France*

12 ^d *LPG, UMR CNRS 6112, Laboratoire de Planétologie et Géodynamique de Nantes,*
13 *Université de Nantes, 44322 Nantes cedex 03, France*

14 ^e *Université Lumière – Lyon 2, UMR CNRS 5133 ArchéOrient, Lyon, France*

15 ^f *Institute of Physics of the Earth, Russian Academy of Science, Moscow, Russia*

16
17

18 *Keywords:* Archeomagnetism, Geomagnetic field intensity, Neolithic, Halaf, Middle East,
19 Holocene

20

21 **ABSTRACT**

22 We present new archeomagnetic intensity data from two Late Neolithic archeological
23 sites (Tell Halula and Tell Masaikh) in Syria. These data, from 24 groups of potsherds
24 encompassing 15 different time levels, are obtained using the Triaxe experimental
25 protocol, which takes into account both the thermoremanent magnetization anisotropy
26 and cooling rate effects on intensity determinations. They allow us to recover the
27 geomagnetic intensity variations in the Middle East, between ~7000 BC and ~5000 BC,
28 i.e. during the so-called pre-Halaf, proto-Halaf, Halaf and Halaf-Ubaid Transitional
29 cultural phases. The data are compared with previous archeointensity results of similar
30 ages from Northern Iraq (Yarim Tepe II and Tell Sotto) and Bulgaria. We find that
31 previous dating of the Iraqi material was in error. When corrected, all northern
32 Mesopotamian data show a relatively good consistency and also reasonably match with
33 the Bulgarian archeointensity dataset. Using a compilation of available data, we
34 construct a geomagnetic field intensity variation curve for the Middle East
35 encompassing the past 9000 years, which makes it presently the longest known regional
36 archeomagnetic intensity record. We further use this compilation to constrain variations

37 in dipole field moment over most of the Holocene. In particular, we discuss the
38 possibility that a significant dipole moment maximum occurred during the third
39 millennium BC, which cannot easily be identified in available time-varying global
40 geomagnetic field reconstructions.

41

42 **1. Introduction**

43 Recent studies have been focused on the construction of time-varying global
44 archeomagnetic field models that cover most of the Holocene (e.g. Korte et al., 2011;
45 Nilsson et al., 2014; Pavón-Carrasco et al., 2014). These models have been developed
46 with the aim to decipher core dynamics over centennial and millennial time scales, the
47 evolution of the past solar activity and the interactions between geomagnetic field and
48 external processes (e.g. Korte et al., 2009; Licht et al., 2013; Usoskin et al., 2014). In all
49 these studies, however, the authors acknowledge the fact that for the more ancient
50 periods, i.e. beyond the first millennium BC, the reliability and accuracy of the
51 geomagnetic field models are strongly penalized by the low number and the poor
52 temporal and geographical distributions of the available archeomagnetic and volcanic
53 paleomagnetic data. To overcome this problem, often paleomagnetic data from
54 sediments have been included in the models reference dataset; nevertheless
55 sedimentary data do not significantly improve the accuracy of the models because a part
56 of them, difficult to estimate, may be biased by experimental errors and/or because
57 these data often lack precise dating (e.g. Valet et al., 2008; Nilsson et al., 2010). There is
58 therefore a critical need for new well dated archeomagnetic data dated with ages older
59 than the first millennium BC.

60 The Middle East, thanks to its rich archeological and historical heritage, offers the
61 possibility to travel back through the geomagnetic field history over most of the
62 Holocene, recovering what could be the longest known archeomagnetic field record.
63 Archeomagnetic studies conducted up to now were mainly focused on the Bronze and
64 Iron Age archeological periods, allowing a better characterization of the regional
65 geomagnetic field intensity behavior for the last 3 millennia BC (i.e. Genevey et al., 2003;
66 Gallet and Le Goff, 2006; Gallet et al., 2008, 2014; Ben-Yosef et al., 2008, 2009; Gallet and
67 Al Maqdissi, 2010; Thébaud and Gallet, 2010; Shaar et al., 2011; Ertepinar et al., 2012;
68 Gallet and Butterlin, 2014). These studies have revealed significant field intensity

69 variations, and in particular a series of intensity maxima between ~2600 and 2500 BC,
70 between ~2300-2000 BC, around 1500 BC and at the very beginning of the first
71 millennium BC (e.g. Gallet et al., 2014). These studies have further shown that the
72 beginning of the first millennium BC was most probably marked by the highest
73 geomagnetic field intensity so far detected during the Holocene and perhaps even before
74 (Ben-Yosef et al., 2009; Shaar et al., 2011; Ertepinar et al., 2012; Livermore et al., 2014).

75 In contrast, for older periods between ~7000 BC and 3000 BC, i.e. during the Late
76 Neolithic (or Pottery Neolithic) and the Chalcolithic, the archeointensity data from the
77 Middle East remain relatively scarce, which prevents an accurate description of the
78 regional geomagnetic field intensity variations (e.g. Genevey et al., 2003; Ben-Yosef et al.,
79 2008). However, several possibilities exist to sample pre-Bronze Age archeological sites.
80 This is particularly true for the 6th millennium BC, which saw the development of the
81 Halaf culture throughout the northern Mesopotamian region. This culture was named
82 after the Tell Halaf archeological site in northern Syria (Fig. 1a), which was discovered
83 and first excavated by the German diplomat Max von Oppenheim at the beginning of the
84 20th century. The Halaf culture is notably characterized by a plentiful pottery
85 production presenting a fine and light-colored clay paste, with brown or black
86 monochrome or polychromatic painted decorations (e.g. Akkermans and Schwartz,
87 2003; Nieuwenhuys et al., 2013 and references therein). This well-fired ceramic
88 production thus constitutes a promising target for archeointensity investigations.

89 Going further back in time, archeomagnetic studies may benefit from recent
90 archeological studies conducted in Syria that focused on the 7th millennium BC, which
91 saw the emergence of the first pottery production in the Near East (e.g. Tsuneki and
92 Miyake, 1996; Le Mière and Picon, 1998; Nishiaki and Le Mière, 2005; Molist et al., 2007;
93 Nieuwenhuys et al., 2010, 2013). At first rare, the pottery was sometimes of a
94 surprisingly elaborated conception with a painted decoration during a primitive phase
95 referred to as the "Initial Pottery Neolithic" (~7000-6700 BC; e.g. Van der Plicht et al.,
96 2011). By the middle of the 7th millennium BC, the use of ceramics spread over northern
97 Mesopotamia (Nieuwenhuys et al., 2010, 2013 and references therein). This pre-Halaf
98 period is mainly represented by undecorated plant-tempered pottery with a coarse clay
99 paste shaped into baskets. The fineness of the clay paste improved at the end of the 7th
100 millennium BC during a period referred to as proto-Halaf (~6050-5900 BC), just

101 preceding the Halaf period, with the use of mineral-tempered clay (e.g. Cruells and
102 Nieuwenhuysse, 2004). According to Akkermans and Schwarz (2003), the pre-Halaf
103 coarse pottery was produced in open fires, with heating temperatures of about 700-
104 750°C, while the elaborate Halaf ceramics were most probably heated at higher
105 temperatures in chambered kilns. For the pre- and proto-Halaf periods encompassing
106 the 7th millennium BC, archeointensity studies are thus still possible, but they may be
107 further complicated by the characteristics of the ceramic production.

108 To extend the Syrian geomagnetic field intensity record, which presently mainly
109 documents the Bronze and Iron Age periods, we conducted an archeomagnetic study on
110 the pre-Halaf, proto-Halaf, Halaf and Halaf-Ubaid Transitional archeological periods, a
111 time interval of nearly two millennia (~7000 to ~5000 BC) covering the Pottery
112 Neolithic, at the end of the Neolithic (e.g. Campbell, 2007; Campbell and Fletcher, 2010;
113 Van der Plicht et al., 2011; Nieuwenhuysse et al., 2013 and references therein). The new
114 archeointensity data reported in this study were mostly obtained from potsherds
115 collected from the archeological site of Tell Halula located in northern Syria (Fig. 1a).
116 These results were complemented by few data obtained from potsherds discovered at
117 the archeological site of Tell Masaikh, located south-east along the middle course of the
118 Euphrates river (Fig. 1a). It is of interest to note that the longest and almost continuous
119 regional archeointensity record presently available was obtained from Bulgaria
120 (Kovacheva et al., 2014). It begins around 6000 BC, i.e. a date during the proto-Halaf
121 period, which means that some of the new data presented in this study are the oldest
122 archeointensity data recovered until now. Furthermore, we recall the recent effort of
123 data compilation of archeomagnetic, volcanic and sedimentary paleomagnetic results
124 that led to the construction of global archeomagnetic field models encompassing almost
125 the entire Holocene (Korte et al., 2011; Nilsson et al., 2014; Pavón-Carrasco et al., 2014).
126 Any new archeomagnetic intensity data dated to the Late Neolithic-Early Chalcolithic
127 period, now rather rare (e.g. Genevey et al., 2008; Knudsen et al., 2008), will therefore
128 allow us to test, at least regionally, the accuracy of the available models and in return
129 will better constrain these models. This point is particularly critical and we will also
130 report in this study on erroneous dating of a relatively large archeointensity dataset
131 previously obtained in the Middle East for the 7th and 6th millennia BC (Nachasova and
132 Burakov, 1995, 1998).

133

134 **2. Archeomagnetic sampling**135 *2.1. Tell Halula*

136 Tell Halula ($\lambda=36^{\circ}25'N$, $\varphi=38^{\circ}10'E$) is located in the modern Syrian
137 administrative province of Raqqqa, about 80 km west of the city of Raqqqa and 85 km east
138 of the city of Aleppo. This archeological site, ~4 km west of the Euphrates, forms a sub-
139 circular artificial mound (360 m x 300 m), with an archeological deposit thickness of
140 ~14 m (Fig. 1b). Archeological excavations conducted since 1991 by a team of the
141 Universitat Aut3noma de Barcelona revealed a total of 38 phases of occupation. From
142 the stratigraphic and archeological constraints (including chipped stone artefacts,
143 pottery typology, figurines and architecture), it has been determined that the site was
144 occupied continuously from the Middle Pre-Pottery Neolithic B (PPNB) to the Late Halaf
145 periods, i.e. from ~7800 to 5300 cal BC (Molist et al. 2007, 2013; Molist 1996, 2001).
146 The systematic archeological fieldwork at Tell Halula has brought significant knowledge
147 about the development of farming, especially in the final stages of the Neolithisation
148 process, when economic, technological and cultural changes were being consolidated.

149 The different phases of human occupation have been recovered in several
150 sectors, especially in the south, south-east and central parts of the settlement (Sectors 1,
151 2, 7, 14, 30, 44 and 45). The Neolithic ceramic horizon encompasses most of the seventh
152 millennium BC and part of the sixth millennium BC (Architectural Phases 20 to 38),
153 spanning the pre-Halaf (or Period 5 according to Lyon's School terminology; Hours et al.,
154 1994), the proto-Halaf or Halaf Transitional and the Halaf (Early, Middle, Late) periods.
155 The archeological and stratigraphic data indicate the presence of a sedentary
156 population, with several large houses or architectural structures relatively dispersed
157 over a surface of ~6 ha, i.e. with large open areas between households and buildings for
158 domestic use. Furthermore, several structures for a collective use were discovered for
159 the pre-Halaf period, with a massive enclosing wall in Sector 1 and a drainage channel in
160 Sector SS7 (Molist, 1996, 1998; Molist and Faura, 1999; Molist et al., 2013).

161 The pottery assemblages analyzed in the present study were sampled following
162 the main chronocultural phases documented at Tell Halula (Fig. 2; see description in
163 Molist et al., 2013 and Supplementary Text1). Here, we used the same chronological

164 time scale as in Molist et al. (2013). For the first pottery production within the Early Pre-
165 Halaf (Ceramic Phase I; ~7000-6600 BC), two groups of fragments collected from the
166 top of Sector 2 were analyzed. The first group of fragments (SY 127) was recovered from
167 a pit located in an open area and the second (SY 125), a little younger than the previous
168 one, was collected from an occupation level associated with a rectangular building. For
169 the intermediate pre-Halaf period (Ceramic Phase II; ~6600-6300 BC), three pottery
170 groups were collected from a large outdoor space between several domestic units. Their
171 age assignment was established via stratigraphy, with the group of potsherds SY96
172 being the most recent, SY97-129 intermediate and SY98-128 being the oldest. Finally,
173 pottery group SY130, comprising pottery fragments found in a pit from Sector 49, comes
174 from the late pre-Halaf (Ceramic Phase III; ~6300-6050 BC).

175 For the period referred to as proto-Halaf (~6050-5900 BC), corresponding to
176 Ceramic Phase IV defined at Tell Halula, two pottery groups of household artifacts were
177 collected in Sectors 44 (SY94-137) and 40 (SY95). A single group (SY91) lies within the
178 Early Halaf period (Ceramic Phase V; ~5900-5750 BC), which was recovered from a
179 multicellular house located in sector 44. Different pits discovered in the same area of
180 Sector 45 yielded four contemporaneous groups of pottery (SY87, SY88, SY89, SY90)
181 dated within the Middle Halaf period (Ceramic Phase VI; ~5750-5550 BC).

182 Nine groups of fragments were collected from the most recent chronological
183 phases at Tell Halula dated in the Late Halaf (Ceramic Phase VII; ~5550-5300 BC). This
184 relatively dense sampling was possible due to a relatively complete stratigraphic
185 sequence from Sector 49 (Gómez, 2011). For most of these groups, the fragments were
186 recovered from different pits excavated in a large open yard, that were used for the
187 disposal of ash and domestic waste. The stratigraphic data and the ceramic typology
188 distinguish five successive temporal intervals, each being documented by one or several
189 pottery groups (from older to younger: SY86-131; SY135; SY84 and SY138; SY82 and
190 SY83-136; SY80, SY81 and SY132).

191 In summary, 22 different pottery groups from 14 successive occupation levels
192 were thus sampled at Tell Halula, whose dates span ~1700 years, between ~7000 and
193 ~5300 BC. For displaying the results in a relative chronological framework for phases II
194 and VII, we made the rough approximation of an equi-temporal distribution for
195 respectively the three and five successive occupation levels (i.e. assuming a duration of

196 100 years for each intermediate pre-Halaf level between 6600 BC and 6300 BC and a
197 duration of 50 years for each Late Halaf level between 5550 BC and 5300 BC; dating
198 with * in Table 1).

199

200 2.2. Tell Masaikh

201 The archeological site of Tell Masaikh ($\lambda=34^{\circ}25'N$, $\varphi=40^{\circ}01'E$) is located on a
202 river terrace in the middle Euphrates Valley (left bank), in the modern province of Deir
203 ez-Zor (eastern Syria). Discovered in 1996 by the *Mission Archéologique Française de*
204 *Ashara/Terqa* led by O. Rouault, excavations at Tell Masaikh (~4 km from Terqa),
205 conducted under the leadership of M.-G. Masetti-Rouault, have revealed several phases
206 of occupation starting with the Late Neolithic (Halaf). More recent periods include
207 significant Neo-Assyrian remains, with a citadel and a palace dated in the 9th-8th
208 centuries BC (Iron Age period), which led the identification of Tell Masaikh as the
209 Assyrian city named Kar-Assurnasirpal (see general discussion in Masetti-Rouault,
210 2010).

211 The discovery in the western sector D of Tell Masaikh of an artisanal Halaf
212 settlement makes this site also quite unique. It is located away from most other known
213 Halaf archeological sites situated more to the North with rainfall above 250 mm/year
214 (while rainfall is below this isohyet in the Tell Masaikh region; e.g. Masetti-Rouault,
215 2006; Robert, 2010), which opens discussion on farming systems and on the use of
216 irrigation at this time.

217 Excavations of the Halaf levels at Tell Masaikh unearthed several occupation
218 levels in open areas with fire places (tannurs), several kilns probably for pottery
219 production and a 1.5 m-thick, ~20 m-long stone wall that supported a terrace. A rich
220 ensemble of Late Halaf potsherds was also recovered. The potsherds analyzed in the
221 present study were found in the uppermost layers dated in the Halaf-Ubaid Transitional
222 (~5300-5000 BC; e.g. Campbell and Fletcher, 2010) based on their typology and from
223 the painted decoration that used manganese pigments for black color. The youngest
224 Halaf pottery belongs to polychrome Late Halaf types associated with some Impressed
225 Ware known as Dalma types and Ubaid-style ceramics (Masetti-Rouault, 2005; Robert et
226 al., 2008; Robert, 2010). We sampled in Locus K171 two groups of these fragments with

227 fine mineral-tempered clay paste (pottery groups SY37, SY38), the first in the
228 occupation layer referred to as E2, and the second on floor E7 on top of layer E2.

229

230 **3. New archeomagnetic intensity results**

231 All the archeointensity measurements reported in this study were obtained using
232 the experimental protocol developed by Le Goff and Gallet (2004) for the Triaxe
233 magnetometer. The details of this experimental protocol can be found in Le Goff and
234 Gallet (2004) (see also Genevey et al., 2009; 2013; Hartmann et al., 2010; Gallet et al.,
235 2014). We only recall here that it relies on magnetization measurements of a small
236 specimen ($<1\text{cm}^3$) directly carried out at high temperatures and on a sequence of
237 measurements (with successive heating and cooling cycles) automatically performed
238 over a fixed temperature range between a low temperature referred to as T_1 (typically
239 of 150°C) and a high temperature referred to as T_2 (typically between 500°C and 530°C).
240 In the past few years, a relatively large collection of archeointensity data of different
241 ages and of different origins was obtained using the Triaxe, and comparative studies
242 with results derived from more classical methods (i.e. from the Thellier and Thellier's
243 (1959) method as revised by Coe (1967) or from the IZZI version of Thellier and
244 Thellier's (1959) method; e.g. Yu et al., 2004) demonstrated the reliability of the Triaxe
245 intensity data when quality criteria are taken into account. In our study, we use the
246 same quality criteria relative to the intensity determination for a specimen as those
247 described by Genevey et al. (2009) and Hartmann et al. (2010, 2011), and which were
248 also used more recently by Genevey et al. (2013), Gallet et al. (2014) and Gallet and
249 Butterlin (2014) (Supplementary Table 1). In particular, these criteria allow us to
250 eliminate the data that could be biased due to alteration of the magnetic minerals during
251 heating. Moreover, the temperature range over which the intensity determinations are
252 recovered from each specimen is precisely adjusted so that the analyzed magnetization
253 component is univectorial and corresponds to the magnetization acquired during the
254 manufacture of the pottery. Fig. 3 shows two examples of demagnetization behaviors.
255 After the removal of the viscous low-temperature component, the first behavior shows a
256 single magnetization component above $\sim 200^\circ\text{C}$ (SY89-08), while the second behavior
257 reveals two components (SY140-06). In these cases, the temperature range was
258 adjusted above $\sim 200^\circ\text{C}$ and $\sim 340^\circ\text{C}$, respectively for obtaining intensity determinations

259 at the specimen level. Finally, the intensity data should not be affected by the presence
260 of multidomain magnetite grains and they take into account both the thermoremanent
261 magnetization (TRM) anisotropy and cooling rate effects on TRM acquisition (for a
262 thorough discussion on these aspects, see for instance in Le Goff and Gallet, 2004;
263 Genevey et al., 2008, 2009; Hartmann et al., 2010).

264 Our archeointensity analyses were complemented by hysteresis measurements
265 and by isothermal remanent magnetization (IRM) acquisition up to 0.8 T performed at
266 Saint Maur using a laboratory-built inductometer coupled with an electro-magnet. In
267 most cases, two fragments were analyzed for each group of fragments. IRM
268 measurements show very similar behaviors with saturation reached in relatively low
269 magnetic fields ($\sim 0.2\text{-}0.3$ T), indicating the absence of high-coercivity minerals (Fig. 4a).
270 We note that the hysteresis loops are generally not constricted (Fig. 4b-c).
271 Thermomagnetic low-field susceptibility curves obtained using a KLY-3 Kappabridge
272 coupled with a CS3 thermal unit show that the existing magnetic grains have maximum
273 unblocking temperatures below 600°C (Fig. 4d-g). All these magnetic properties indicate
274 that the magnetization of our specimens is most probably predominantly carried by
275 minerals of the (titano)magnetite family. Furthermore, the thermomagnetic curves
276 exhibit variable behaviors, independently of the age of the fragments, which suggests
277 the presence of (titano)magnetite with different titanium contents or different grain
278 sizes. We also observe a good reversibility between the heating and cooling
279 susceptibility vs. temperature curves, which constitutes a good marker of the stability of
280 the magnetic mineralogy on heating. We note that these magnetic properties are very
281 similar to those we previously obtained from Syrian fired-clay artifacts of younger ages
282 (e.g. Genevey et al., 2003; Gallet et al., 2008; 2014; Gallet and Butterlin, 2014).

283 Except for one case, the hysteresis parameters obtained for the fragments from
284 Tell Halula lie within the pseudo-single domain (PSD) range of magnetite defined by
285 Dunlop et al. (2002a) when projected on a Day plot (Day et al., 1977). Most M_{RS}/M_S and
286 H_{CR}/H_C ratios are concentrated inside a restricted area, with $\sim 0.30 > M_{RS}/M_S > \sim 0.15$ and
287 $\sim 4 > H_{CR}/H_C > \sim 2.5$), above the theoretical mixing curves for mixture of SD and MD
288 magnetite grains but also well below the mixing curve of SD and superparamagnetic
289 (SP) magnetite grains (Fig. 4h). According to Dunlop (2002b), this may reflect a large
290 distribution of grain sizes, including SP, SD and MD magnetite grains. In contrast, most

291 of the hysteresis parameters obtained from Tell Masaïkh (open blue triangles in Fig. 4h)
292 fall within the theoretical SD-MD mixing curves defined by Dunlop (2002a), therefore
293 indicating a coarser grain size distribution for those specimens. It is worth mentioning
294 that the evolution of the techniques (preparation of the clay paste, firing conditions)
295 used to produce ceramics at Tell Halula between the pre-Halaf and Halaf periods is
296 clearly not reflected in the hysteresis ratios, their dispersions being very similar
297 regardless of the age of the fragments (colored symbols in Fig. 4h). Further considering
298 the data from Tell Masaïkh and the previous ones obtained from Ebla/Tell Mardikh
299 (grey dots in Fig. 4h; Gallet et al., 2014), it appears that the distribution of the hysteresis
300 parameters obtained at a given archeological site constitutes a magnetic signature of the
301 clay source used to produce pottery at this site, and it may be used as an identification
302 tool complementary to more classical chemical analyses.

303 Fig. 5 shows the intensity results obtained from eight pottery groups. Each curve
304 from each panel shown in this figure exhibits the intensity data obtained for one
305 specimen over a temperature range often exceeding 200-250°C. In general, we only
306 analyzed one specimen per fragment. However, when the number of favorable
307 fragments was ≤ 5 (i.e. for pottery groups SY127, SY125, SY95, SY38), we analyzed three
308 specimens from each fragment and we first estimated a mean intensity value at the
309 fragment level before computing a mean value at the group level. The success rate of our
310 archeointensity analyses significantly varies according to the archeological periods.
311 While it is only 36% for the pre-Halaf period (54 fragments from 151 analyzed
312 fragments) and 56 % (22 from 39 fragments) for the proto-Halaf period, it increases up
313 to 70% for the sites dated in the Halaf period (133 from 191 fragments) and 67% for the
314 Halaf-Ubaid Transitional period (16 favorable fragments from 24 studied fragments).
315 The relatively low success rate for the pre-Halaf fragments is mainly due to the presence
316 of two magnetization components, which is likely related to the use of these ceramics for
317 cooking (hence preventing in many cases the clear isolation of a primary
318 magnetization). Examples of failed results are reported in Supplementary Fig. 1. Overall,
319 we analyzed a total of 405 fragments, among which 225 fragments (254 specimens)
320 yielded favorable archeointensity results, allowing us to determine 24 mean intensity
321 values at the pottery group level. Results obtained at the specimen/fragment level are
322 detailed in Supplementary Table 2, while Table 1 provides the group-mean intensity
323 values. These intensity values are generally well defined, with a number of fragments

324 analyzed per site larger or equal to 7 for 19 pottery groups (≥ 10 for 10 sites) and a
325 standard deviation always of less than 5 μT , ranging between 1.8 % and 11.4 % of the
326 corresponding group-mean intensity values (≤ 5.0 % for 10 sites and ≤ 7.5 % for 21
327 among the 24 studied pottery groups). We note, however, that the mean intensity value
328 obtained for group SY125 (~6650-6550 BC) is only defined by two fragments (6
329 specimens), but it was kept for the discussion below because of the scarcity of such old
330 archeointensity data.

331

332 4. Late Neolithic archeointensity variations in the Middle East

333 The new archeointensity data are reported in Fig. 6 (see also Supplementary Fig.
334 2, where the results are averaged over the successive occupation levels). The new
335 results show that the time interval between ~7000 BC and ~5000 BC was apparently
336 marked in the Middle East by an overall decreasing trend in geomagnetic field intensity.
337 This decrease was however not regular. In particular, a relative intensity minimum is
338 observed at the beginning of the Late Halaf period (pottery group SY86-131 with 20
339 favorable fragments), around the middle of the 6th millennium BC. An intensity peak
340 appears to have occurred during the Late Halaf period, between ~5550 and ~5300 BC.
341 This intensity peak is supported by the low geomagnetic field intensity values obtained
342 at Tell Masaikh for the Halaf-Ubaid Transitional period.

343 We compared the new Tell Halula and Tell Masaikh data with two other
344 archeointensity datasets of the same age previously obtained in relatively nearby
345 regions (Fig. 7). The first dataset includes results obtained at Yarim Tepe II and Tell
346 Sotto, two multi-level archeological sites from northern Iraq (Fig. 1a; Nachasova and
347 Burakov, 1995, 1998). In these two studies, the pottery fragments were selected and
348 dated according to their stratigraphic position within a sequence of archeological
349 deposits (with a total thickness of 780 cm at Yarim Tepe II and 280 cm at Tell Sotto), and
350 assuming a constant accumulation rate of archeological deposits. Although such a
351 sampling procedure may obviously introduce large uncertainties in the dating of the
352 studied fragments, it nevertheless appears that this approach can provide satisfactory
353 results (e.g. Nachasova and Burakov, 1998; Kostadinova-Avramova et al., 2014).
354 However, in both cases, the dating considered by Nachasova and Burakov (1995, 1998)

355 appears systematically shifted by several centuries relative to the most recent
356 chronological Pottery Neolithic time scale (see Campbell, 2007; Bernbeck and
357 Nieuwenhuys, 2013). Indeed, the fragments from Yarim Tepe II are unambiguously
358 archeologically dated to the Middle-Late Halaf period (~5750-5300 BC; e.g., Campbell,
359 2007; Robert, 2009; Bernbeck and Nieuwenhuys, 2013 and references therein), but
360 their ages were mostly assigned in the 5th millennium BC. Similarly, the fragments
361 collected at Tell Sotto were dated to the middle of the 6th millennium BC by Nachasova
362 and Burakov (1998), but the studied ceramics are dated to the Late Pre-Halaf (Late
363 proto-Hassuna and Archaic Hassuna cultural phases), i.e. between ~6400 and ~6050 BC
364 (e.g. Bader, 1989; Bader and Le Mière, 2013; Le Mière pers. comm. 2014).

365 For these reasons, we assigned new ages to Yarim Tepe II and Tell Sotto
366 considering first, the stratigraphic position of the concerned fragments as provided by
367 the authors and second, assuming that the entire Middle-Late Halaf and Late Pre-Halaf
368 periods were represented in the Yarim Tepe II and Tell Sotto deposits (like the authors
369 considered but for two other time intervals). Finally, for displaying in Fig. 7a the data
370 obtained at Yarim Tepe II, with only a single specimen studied per fragment, and at Tell
371 Sotto we also performed intensity averaging over several fragments when the latter
372 come from the same stratigraphic intervals, i.e. each time there was a group of
373 fragments considered of the same age. We observe an overall good agreement with the
374 data obtained at Tell Halula and Tell Masaikh. In particular, this agreement confirms the
375 occurrence in northern Mesopotamia of a relative intensity minimum around the middle
376 of the 6th millennium BC, which further strengthens the occurrence of an intensity peak
377 at the beginning of the second half of the 6th millennium BC.

378 The second archeointensity dataset comprises the results encompassing the 6th
379 millennium BC from Bulgaria that were recently updated by Kovacheva et al. (2014)
380 (Fig. 7b). From this new analysis, a century-scale intensity peak seems to be emerging
381 around the middle of the 6th millennium, which might coincide, within age uncertainties,
382 with that observed from the Syrian Late Halaf data. According to this interpretation, the
383 data available for the Halaf-Ubaid Transitional period would come prior to the
384 geomagnetic field intensity increase observed in the Bulgarian data at the end of the 6th
385 millennium BC. Constraining further this preliminary correlation will require the
386 acquisition of new archeointensity data in the Balkans and in the Middle East.

387

388 **5. Discussion**

389 We have undertaken the construction of a geomagnetic field intensity secular
390 variation curve in the Middle East during the Holocene. For this purpose, we selected all
391 the archeointensity data available inside a circle with a radius 1000 km around the
392 archeological site of Tell Halaf ($\lambda=36^{\circ}49'N$, $\varphi=40^{\circ}02'E$; Supplementary Fig. 3). The data
393 were retrieved from the ArcheoInt database (Genevey et al., 2008) and complemented
394 with the more recent studies (Ben-Yosef et al., 2009; Gallet and Al Maqdissi, 2010; Shaar
395 et al., 2011, 2014; Ertepinar et al., 2012; Gallet et al., 2014; Gallet and Butterlin, 2014).
396 They were obtained from the eastern part of Turkey, Cyprus, Syria, the Levant, Iraq,
397 from the western part of Iran and from the Caucasus. Note that the large dataset from
398 the Balkans and Greece (e.g. De Marco et al., 2008; Tema and Kondopoulou, 2011;
399 Kovacheva et al., 2014) has not been included to allow it to be compared to different
400 regional secular variation behaviors from elsewhere (e.g. between the Middle East,
401 Eastern Europe and Western Europe). Genevey et al. (2008) proposed a set of selection
402 criteria in order to distinguish between all available data those that meet minimum
403 quality criteria. This approach enabled the construction of two datasets referred to as
404 "Selected data" and "All data" in Genevey et al. (2008). Hereafter we have considered the
405 compilation of selected data to calculate the Middle East geomagnetic field intensity
406 variation curve, considering the new dating we estimated for Tell Sotto and Yarim Tepe
407 II and using, for these two sites, the mean intensity values computed from fragments
408 associated with the same stratigraphic level (Fig. 7a).

409 To calculate our curve, we first applied a method based on the use of sliding
410 windows of 200 years successively shifted by 10 years through the past 9 millennia. We
411 computed VADM values only for those time intervals containing at least 3 results.
412 Following Thébaut and Gallet (2010) and Licht et al. (2013), we also used the bootstrap
413 technique with 1000 runs by introducing random noise in the data within their
414 experimental and age uncertainties. This allowed us to compute 1000 intensity variation
415 curves. In Fig. 8a we displayed the averaged VADM (thick line) together with the
416 minimum and maximum VADM values obtained for the different sliding windows, hence
417 defining an envelope of equally possible VADM values. Due to the insufficient number of
418 archeointensity data spanning the 5th and 4th millennia BC, no averaged curve could be

419 determined between ~4930 BC and ~3650 BC, i.e. during the Ubaid and Uruk periods in
420 Mesopotamia. This time interval therefore constitutes a particularly important target for
421 future archeomagnetic studies in the Middle East. For other periods, the computed curve
422 appears very consistent with almost all the Syrian data (blue dots in Fig. 8a; Genevey et
423 al., 2003; Gallet and Le Goff, 2006; Gallet et al., 2006, 2008, 2014; Gallet and Al Maqdissi,
424 2010; Gallet and Butterlin, 2014 and this study). We observe the same variation trends,
425 with distinct intensity maxima during the second half of the first millennium AD, at the
426 beginning of the first millennium BC and around the middle of the third millennium BC.
427 Supplementary Fig. 4 also exhibits the averaged intensity curve computed without the
428 Syrian data, showing in particular that the latter data set allows us to better constrain
429 the curve during the third millennium BC (note that this curve takes into account the
430 new dating of the Tell Sotto and Yarim Tepe II data). The temporal resolution of 200
431 years of the regional averaged curve most probably prevents the recovery of distinct
432 century-scale intensity (VADM) maxima at ~1500 BC, ~2550 BC and ~2300 BC clearly
433 observed from Syrian data at Ebla and Mari (Gallet et al., 2008, 2014; Gallet and
434 Butterlin, 2014), as well as the maximum in intensity between ~5500 and ~5300 BC
435 exhibited by the Tell Halula data or the spike events proposed by Ben-Yosef et al. (2009)
436 and Shaar et al. (2011) at the very beginning of the first millennium BC.

437 The second approach is similar to the method described above but relies on the
438 more complex cubic B-splines time parameterization and uses an iterative scheme to
439 identify and then to weight the data that are considered as outliers (Fig. 8b; modified
440 from Thébault and Gallet, 2010). The algorithm first proposes a set of possible spline
441 knots irregularly spaced. The spacing is designed to take full advantage of the varying
442 time resolution between epochs that arises from the uneven time distribution of the
443 reference archeomagnetic data. For instance, it is found that the maximum achievable
444 time resolution is about 150 years between 7000 BC to about 5000 BC and between
445 ~3000 BC and 2000 AD, while searching for features with time resolution lower than
446 800 years makes little sense between ~5000 BC and ~3000 BC. Then, the data are as
447 before 1000 times randomly noised within their a priori error bars. For each curve, the
448 algorithm checks whether the maximum likelihood solution belongs to the a priori 95%
449 error bar of the data and weights accordingly the data that are systematically outside
450 this confidence interval. Fig. 8b displays the final solution with the maximum probability

451 in black and its 95% fluctuation envelope in light blue. This envelope contains 95% of
452 the maximum likelihood curves estimated by the bootstrap for the 1000 iterations, and
453 it highlights the variability between the different curves. This parameter is important for
454 testing the precision of the most probable curve and for identifying the fine time
455 variations that persist after resampling. Formally, however, the statistical significance of
456 a time variation can be assessed only after the computation of the 95% confidence
457 interval (in red) that is traditionally calculated *a posteriori* from the misfit function
458 between the data and the ensemble of models. Compared to the first approach, the
459 likelihood solution provided in supplementary Table 3 is generally smoother. This
460 feature is desired for testing whether the apparent fine time variation of the maximum
461 likelihood can be considered as robust. A striking feature emerging from the comparison
462 between Fig. 8a and Fig. 8b is that the final solution is independent of the chosen
463 modeling scheme. This is seemingly positive evidence that the observed magnetic field
464 intensity variations are well constrained (within the given time resolution) by the
465 available data in the chosen geographical area.

466 We then sought to constrain the variations in global geomagnetic dipole field
467 moment over the past 9 millennia. For this, we averaged the archeointensity data
468 available in the Middle East over sliding windows of 500 years, roughly assuming that
469 this rather long duration may suffice to average out most of the non-dipole
470 contributions (e.g. Hulot and Le Mouél, 1994; Genevey et al., 2008; Knudsen et al., 2008).
471 On the other hand, this averaging smoothes out the more rapid variations in dipole
472 moment over centennial time scales (Genevey et al., 2009; 2013). The curve constructed
473 using the same technique as in Fig. 8a is shown in Fig. 9a, together with the VADM
474 computed by Knudsen et al. (2008) using the global GEOMAGIA50 database (Korhonen
475 et al., 2008) and applying both temporal and geographical averaging to eliminate the
476 non-dipole components. As a general comment, the two curves exhibit the same dipole
477 behavior during the past three millennia (although the magnitude and the amplitude of
478 the variations are not strictly the same), characterized by two periods of stronger dipole
479 moment during the first millennium BC and during the second half of the first
480 millennium AD (see also Genevey et al., 2008; Hong et al., 2013). In contrast, these
481 curves are significantly different during the third millennium BC, with a smooth VADM
482 evolution in the case of the Knudsen et al. (2008) curve but with a distinct dipole
483 maximum in our Middle East curve. For older periods, there is again a good consistency

484 between the two curves, but we note the large error bars of Knudsen et al.'s (2008)
485 curve for the 7th-6th millennium segment. Thus the question remains as to the
486 significance of the dipole maximum observed in the Middle East during the third
487 millennium BC, which is well constrained by a significant number of data. Owing to the
488 rather good agreement between the two curves, especially during the past three
489 millennia, the VADM maximum we observe during the third millennium BC might well
490 be a global (dipole) geomagnetic feature that requires further confirmation. If true, it
491 would indicate that the dipole evolution varied more erratically than previously thought,
492 with an oscillatory behavior at least between ~3000 BC and 2000 AD of typical time
493 scale of about 1700 years (see also Burakov et al., 1998).

494 Fig. 9b compares our VADM variation curve with dipole moments derived from
495 global geomagnetic field modeling that was recently constructed using only
496 archeomagnetic and volcanic data (Pavón-Carrasco et al., 2014, in blue) and another that
497 also incorporated paleomagnetic data from sediments (Nilsson et al., 2014 in orange and
498 green; note that this latter reconstruction supersedes the previous field reconstruction
499 of Korte et al., 2011). The field models that partly rely on sediment data naturally show
500 time variations smoother than that of the models constructed using only the
501 archeomagnetic and volcanic data. Hence, the dipole moments derived by Nilsson et al.
502 (2014) during the 7th millennium BC are lower than the ones proposed by Pavón-
503 Carrasco et al. (2014) and lower than the averaged VADM we estimated from the Middle
504 East. However, at the beginning of the first millennium BC, the VADM values from the
505 Middle East are much higher than the dipole moments from either models. Neither of
506 two reconstructions shows the distinct dipole maxima previously observed during the
507 past three millennia (Fig. 9a; Genevey et al., 2008; Knudsen et al., 2008), in particular the
508 one dated to the first millennium AD. This clearly poses the question of the consistency
509 between the VADM estimates and the time-varying dipole moment reconstructions.
510 Nevertheless, it could be argued that the field modeling of Pavón-Carrasco et al. (2014)
511 gives some support to the occurrence of a dipole moment maximum during the third
512 millennium BC (Fig. 9b). Such an agreement still needs to be confirmed because the
513 proposed field reconstruction shows numerous centennial-scale fluctuations with
514 similar amplitudes over the entire sequence, a feature whose geomagnetic origin is
515 questionable.

516 As a concluding remark, we point out that the different time-varying
517 archeomagnetic field reconstructions encompassing the 7th-5th millennium time
518 interval all suffer from the erroneous dating affecting the Yarim Tepe II and Tell Sotto
519 data. Together with the corrected Yarim Tepe II and Tell Sotto ages, the new
520 archeointensity data obtained in the present study dated to between 7000 BC and 5000
521 BC will help improve the reliability of the next generation of geomagnetic field models
522 spanning the Late Neolithic period. Besides implications for geomagnetism, this
523 improvement may be of particular interest in providing chronological time constraints
524 for archeological purposes, during a fascinating period (e.g. Berger and Guilaine, 2009)
525 that was marked by the beginning of the Neolithic expansion from the Middle East
526 toward Western Europe.

527

528 **Acknowledgements**

529 We thank Michel Al Maqdissi (DGAM, Damascus), who made possible this
530 archeomagnetic study. We are also grateful to Stuart Gilder and 2 anonymous reviewers
531 for helpful comments on the manuscript. Y.G. and I.N. were partly financed by grant of
532 the Russian Ministry of Science and Education N 14.Z50.31.0017. IPGP contribution no.
533 Xxx

534

535 **References**

- 536 Akkermans, P.M.M.G., Schwartz, G.M., 2003. The archaeology of Syria. From complex
537 hunter-gatherers to early urban societies (ca. 16,000-300 BC). Cambridge World
538 Archaeology, Cambridge University Press, New York, 467 pp.
- 539 Bader, N., 1989. Earliest Cultivators in Northern Mesopotamia. The Investigations of
540 Soviet Archaeological Expedition in Iraq at Settlements Tell Magzaliya, Tell Sotto,
541 Kül Tepe. Moscow, Nauka.
- 542 Bader, N., Le Mière, M., 2013. From pre-Pottery Neolithic to Pottery Neolithic in the
543 Sinjar, in *Interpreting the Late Neolithic of Upper Mesopotamia*. Publications on
544 Archaeology of the Leiden Museum of Archaeology (PALMA), Brepols pub.
545 (Turnhout, Belgium), 513-520.

- 546 Bernbeck, J., Nieuwenhuysse, O.P., 2013. Established paradigms, current disputes and
547 emerging themes: the state of research on the Late Neolithic in Upper
548 Mesopotamia, in *Interpreting the Late Neolithic of Upper Mesopotamia*.
549 *Publications on Archaeology of the Leiden Museum of Archaeology (PALMA)*,
550 Brepols pub. (Turnhout, Belgium), 17-37.
- 551 Ben-Yosef, E., Ron, H., Tauxe, L., Agnon, A., Genevery, A., Levy, T.E., Avner, U., Najjar, M.,
552 2008. Application of copper slag in geomagnetic archaeointensity research. *J.*
553 *Geophys. Res.* 113, B08101. doi:10.1029/2007JB005235.
- 554 Ben-Yosef, E., Tauxe, L., Levy, T.E., Shaar, R., Ron, H., Najjar, M., 2009. Geomagnetic
555 intensity spike recorded in high resolution slag deposit in southern Jordan. *Earth*
556 *Planet. Sci. Lett.* 287, 529-539.
- 557 Berger, J.-F., Guilaine, J., 2009. The 8200 calBP abrupt environmental change and the
558 Neolithic transition: A Mediterranean perspective. *Quaternary Int.* 200, 31-49.
- 559 Burakov, K.S., Galyagin, D.K., Nachasova, I.E., Reshetnyak, M. Yu., Sokolov, D.D., Frick,
560 P.G., 1998. Wavelet analysis of geomagnetic field intensity for the past 4000 years.
561 *Izvestiya Phys. of Solid Earth* 34 (9), 773-778.
- 562 Campbell, S., 2007. Rethinking Halaf chronology. *Paléorient* 33, 103-136.
- 563 Campbell, S., Fletcher, A., 2010. Questioning the Halaf-Ubaid Transition. In: *Beyond the*
564 *Ubaid: Transformation and integration in the late prehistoric societies of the*
565 *Middle East*, R.A. Carter and G. Philip eds., SAOC: Studies in Ancient Oriental
566 *Civilization* 63, The Oriental Institute of the University of Chicago, 69-83.
- 567 Coe, R. S., 1967. Paleo-Intensities of the Earth's magnetic field determined from Tertiary
568 and Quaternary Rocks. *J. Geophys. Res.* 72, 3247-3262.
- 569 Cruells, W., Nieuwenhuysse, O., 2004. The proto-Halaf period in Syria. New sites, new
570 data. *Paléorient* 30, 47-68.
- 571 Day, R., Fuller, M., Schmidt, V., 1977. Hysteresis properties of titanomagnetites: grain
572 size and composition dependence. *Phys. Earth Planet. Inter.* 13, 260-267.
- 573 De Marco, E., Spatharas, V., Gomez-Paccard, M., Chauvin, A., Kondopoulou, D., 2008. New
574 archeointensity results from archeological sites and variations of the geomagnetic
575 field intensity for the last 7 millennia in Greece. *Phys. Chem. Earth* 33, 578-595.

- 576 Dunlop, D.J., 2002a. Theory and application of the Day plot (Mrs/Ms versus Hcr/Hc) 1.
577 Theoretical curves and tests using titanomagnetite data. *J. Geophys. Res.* 107, 2056,
578 10.1029/2001JB000486.
- 579 Dunlop, D.J., 2002b. Theory and application of the Day plot (Mrs/Ms versus Hcr/Hc) 2.
580 Application to data for rocks, sediments, and soils. *J. Geophys. Res.* 107, 2057,
581 10.1029/2001JB000487.
- 582 Ertepinar, P., Langereis, C.G., Biggin, A.J., Frangipane, M., Matney, T., Ökse, T., Engin, A.,
583 2012. Archaeomagnetic study of five mounds from Upper Mesopotamia between
584 2500 and 700 BC: further evidence for an extremely strong geomagnetic field ca.
585 3000 years ago. *Earth Planet. Sci. Lett.* 357-358, 84-98.
- 586 Gallet, Y., Le Goff, M., 2006. High-temperature archeointensity measurements from
587 Mesopotamia. *Earth Planet. Sci. Lett.* 241, 159-173.
- 588 Gallet, Y., Genevey, A., Le Goff, M., Fluteau, F., Eshraghi, S.A., 2006. Possible impact of the
589 Earth's magnetic field on the history of ancient civilizations. *Earth Planet. Sci. Lett.*
590 246, 17-26.
- 591 Gallet, Y., Le Goff, M., Genevey, A., Margueron, J., Matthiae, P., 2008. Geomagnetic field
592 intensity behavior in the Middle East between 3000 BC and 1500 BC. *Geophys. Res.*
593 *Lett.* 35, L02307. doi: 10.1029/2007GL031991.
- 594 Gallet, Y., Genevey, A., Le Goff, M., Warmé, N., Gran-Aymerich, J., Lefèvre A., 2009a. On the
595 use of archeology in geomagnetism, and vice-versa: Recent developments in
596 archeomagnetism. *C. R. Physique* 10, 630-648.
- 597 Gallet, Y., Hulot, G., Chulliat, A., Genevey, A., 2009b. Geomagnetic field hemispheric
598 asymmetry and archeomagnetic jerks. *Earth Planet. Sci. Lett.* 284, 179-186.
- 599 Gallet, Y., D'Andrea, M., Genevey, A., Pinnock, F., Le Goff, M., Matthiae, P., 2014.
600 Archaeomagnetism at Ebla (Tell Mardikh, Syria). New data on geomagnetic field
601 intensity variations in the Near East during the Bronze Age. *J. Archaeol. Sci.* 42,
602 295-304.
- 603 Gallet, Y., Butterlin, P., 2014. Archaeological and geomagnetic implications of new
604 archaeomagnetic intensity data from the Early Bronze high terrace "Massif Rouge"

- 605 at Mari (Tell Hariri, Syria). *Archaeometry* online 5 June 2014, doi:
606 10.1111/arcm.12112.
- 607 Gallet, Y., Al Maqdissi, M., 2010. Archéomagnétisme à Mishirfeh-Qatna: Nouvelles
608 données sur l'évolution de l'intensité du champ magnétique terrestre au Moyen-
609 Orient durant les derniers millénaires. *Akkadica* 131, 29-46.
- 610 Genevey, A., Gallet, Y., 2002. Intensity of the geomagnetic field in Western Europe over
611 the past 2000 years: New data from ancient French pottery. *J. Geophys. Res.* 107,
612 B11.
- 613 Genevey, A., Gallet, Y., Margueron, J., 2003. Eight thousand years of geomagnetic field
614 intensity variations in the eastern Mediterranean. *J. Geophys. Res.* 108, 2228.
615 doi:10.1029/2001JB001612.
- 616 Genevey, A., Gallet, Y., Constable, C., Korte, M., Hulot, G., 2008. ArcheoInt: An upgraded
617 compilation of geomagnetic field intensity data for the past ten millennia and its
618 application to the recovery of the past dipole moment. *Geochem. Geophys. Geosyst.*
619 9(4), Q04038. doi: 10.1029/2007GC001881.
- 620 Genevey, A., Gallet, Y., Rosen, J., Le Goff, M., 2009. Evidence for rapid geomagnetic field
621 intensity variations in Western Europe over the past 800 years from new
622 archeointensity French data. *Earth Planet. Sci. Lett.* 284, 132-143.
623 doi:10.1016/j.epsl.2009.04.024.
- 624 Genevey, A., Gallet, Y., Thébaud, E., Jesset, S., Le Goff, M., 2013. Geomagnetic field
625 intensity variations in Western Europe over the past 1100 years. *Geochem.*
626 *Geophys. Geosyst.* 14/8, 2858-2872
- 627 Gómez, A., 2011. Caracterización del producto cerámico en las comunidades neolíticas
628 de mediados del VI milenio cal BC: el valle del Éufrates y el valle del Khabur en el
629 Halaf Final. PhD Thesis, Universitat Autònoma de Barcelona, Spain.
- 630 Hartmann, G., Genevey, A., Gallet, Y., Trindade, R., Etchevarne, C., Le Goff, M., Afonso, M.,
631 2010. Archeointensity in Northeast Brazil over the past five centuries. *Earth*
632 *Planet. Sci. Lett.* 296, 340-352.
- 633 Hartmann, G., Genevey, A., Gallet, Y., Trindade, R., Le Goff, M., Najjar, R., Etchevarne, C.,
634 Afonso, M., 2011. New historical archeointensity data from Brazil : Evidence for a

- 635 large regional non-dipole field contribution over the past few centuries. Earth
636 Planet. Sci. Lett. 306, 66-76.
- 637 Hong, H., Yu, Y., Lee, C.H., Kim, R.H., Park, J., Doh, S.-J., Kim, W., Sung, H., 2013. Globally
638 strong geomagnetic field intensity circa 3000 years ago. Earth Planet. Sci. Lett. 383,
639 142-152.
- 640 Hours, F., Aurenche, O., Cauvin, J., Cauvin, M.C., Copeland, L., Sanlaville, P., 1994. Atlas des
641 sites du Proche-Orient (14000-5700 BP). Travaux de la Maison de l'Orient
642 Méditerranéen 24, Lyon.
- 643 Hulot, G., Le Mouél, J.-L., 1994. A statistical approach to the Earth's main magnetic field.
644 Phys. Earth Planet. Inter. 82, 167-183.
- 645 Knudsen, M., Riisager, P., Donadini, F., Snowball, I., Muscheler, R., Korhonen, K., Pesonen,
646 L., 2008. Variations in geomagnetic dipole moment during the Holocene and the
647 past 50 kyr. Earth Planet. Sci. Lett. 272, 319-329.
- 648 Korhonen, K., Donadini, F., Riisager, P., Pesonen, L.J., 2008. GEOMAGIA50: An
649 archeointensity database with PHP and MySQL. Geochem. Geophys. Geosyst. 9,
650 Q04029.
- 651 Korte, M., Donadini, F., Constable, C., 2009. Geomagnetic field for 0-3 ka: 2. A new series
652 of time-varying global models. Geochem. Geophys. Geosyst. 10, Q06008.
- 653 Korte, M., Constable, C., Donadini, F., Holme, R., 2011. Reconstructing the Holocene
654 geomagnetic field. Earth Planet. Sci. Lett. 312, 497-505.
- 655 Kostadinova-Avramova, M., Kovacheva, M., Boyadzhiev, Y., 2014. Contribution of
656 stratigraphic constraints of Bulgarian prehistoric multilevel tells and a comparison
657 with archaeomagnetic observations. J. Archaeol. Sci. 43, 227-238.
- 658 Kovacheva, M., Kostadinova-Avramova, M., Jordanova, N., Lanos, P., Boyadzhiev, Y., 2014.
659 Extended and revised archaeomagnetic database and secular variation curves from
660 Bulgaria for the last eight millennia. Phys. Earth Planet. Inter. In press, doi:
661 10.1016/j.pepi.2014.07.002.
- 662 Le Goff, M., Gallet, Y., 2004. A new three-axis vibrating sample magnetometer for
663 continuous high-temperature magnetization measurements: applications to paleo-
664 and archeo-intensity determinations. Earth Planet. Sci. Lett. 229, 31-43.

- 665 Le Mière, M., Picon, M., 1998. Les débuts de la céramique du Proche-Orient. *Paléorient*
666 24/2, 27-48.
- 667 Licht, A., Hulot, G., Gallet, Y., Thébault, E., 2013. Ensembles of low degree archeomagnetic
668 field models for the past three millennia. *Phys. Earth Planet. Inter.* 224, 38-67.
- 669 Livermore, P.W., Fournier, A., Gallet, Y., 2014. Core-flow constraints on extreme
670 archeomagnetic intensity changes, *Earth Planet. Sci. Lett.* 387, 145-156
- 671 Masetti-Rouault, M.-G., 2005. Mission archéologique française à Tell Masaïkh, projet
672 Terqa et sa région. Rapport préliminaire de la mission 2005 à Tell Masaïkh", p. 1-
673 12.
- 674 Masetti-Rouault, M.-G., 2006. Rapporto preliminare sui lavori della missione nel sito di
675 Tell Masaïkh nel 2005 (MK10). In : Rouault O. et Mora C., Progetto Terqa e la sua
676 regione (Siria). Rapporto preliminare 2005, *Athenaeum fasc. 2*, p. 749-756.
- 677 Masetti-Rouault, M.-G., . Rural Economy and Steppe Management in an Assyrian Colony
678 in the West. A view from Tell Masaïkh Lower Middle Euphrates, Syria. In: H. Kühne
679 ed. *Dur-Katlimmu 2008 and Beyond*, *Studia Chaburensia*, vol. 1, Harrassowitz
680 Verlag, 130-149.
- 681 McIntosh, G., Kovacheva, M., Catanzariti, G., Osete, M.L., Casas, L., 2007. Widespread
682 occurrence of a novel high coercivity, thermally stable, low unblocking
683 temperature magnetic phase in heated archeological material. *Geophys. Res. Lett.*
684 34, L21302.
- 685 McIntosh, G., Kovacheva, M., Catanzariti, G., Donadini, F., Lopez, M.L.O., 2011. High
686 coercivity remanence in baked clay materials used in archeomagnetism. *Geochem.*
687 *Geophys. Geosyst.* 12, Q02003, doi:10.1029/2010GC003310.
- 688 Molist, M., 1996 (ed.). Tell Halula (Siria). Un yacimiento neolítico del valle medio del
689 Éufrates. Campañas de 1991 y 1992. Ediciones del Ministerio de Educación y
690 Ciencia, Madrid Spain, 223 p.
- 691 Molist, M., 1998. Espace collectif et domestique dans le néolithique des IXème et VIIIème
692 millénaires B.P. au nord de la Syrie: apports du site de Tell Halula (Vallée de
693 l'Euphrate), in *Espace Naturel, Espace Habité en Syrie du Nord. (10e-2e millénaires*
694 *av. J. C.)*. M. Fortin and O. Aurenche eds., 115-130, Québec-Lyon, BCSMS-TMO.

- 695 Molist, M., Faura, J.M., 1999. Tell Halula: Un village des premiers agriculteurs-éleveurs
696 dans la Vallée de l'Euphrate, in *Archaeology of the Upper Syrian Euphrates. The*
697 *Tishrin Dam Area*, Del Olmo, G. and Montero J. L. (eds.), *Proceedings of the*
698 *International Symposium held at Barcelona, January 28-30 1998*, Ed. Ausa,
699 Sabadell: 27-40.
- 700 Molist, M., 2001. Halula, village néolithique en Syrie du Nord, in *Communautés*
701 *villageoises du Proche-Orient à l'Atlantique (8000-2000 av. J.-C.)*, Guilaine J. (ed),
702 115-130, Paris, Editions Errance.
- 703 Molist, M., Anfruns, J., Borrell, F., Clop, X., Cruells, W., Gómez, A., Guerrero, E., Tornero, C.,
704 Sana, M., 2007. Tell Halula (vallée de l'Euphrate, Syrie): nouvelles données sur les
705 occupations Néolithiques. Notices préliminaires sur les travaux 2002-2004. In *Les*
706 *résultats du programme de formation à la sauvegarde du patrimoine culturel de*
707 *Syrie*, Abdul Massih J. (ed.), 21-52, Damas: Ministère de la culture, Direction
708 générale des antiquités et des musées (Documents d'archéologie syrienne 11).
- 709 Molist, M., Anfruns, J., Bofill, M., Borrell, F., Buxó, R., Clop, X., Cruells, W., Faura, J.M.,
710 Ferrer, A., Gómez, A., Guerrero, E., Saña, M., Tornero, C. & Vicente, O., 2013. Tell
711 Halula (Euphrates Valley, Syria): New approach to VII and VI millennia cal. B.C. in
712 Northern Levant framework, in *Interpreting the Late Neolithic of Upper*
713 *Mesopotamia. Publications on Archaeology of the Leiden Museum of Archaeology*
714 (PALMA), Brepols pub. (Turnhout, Belgium), 443-455.
- 715 Nachasova, I., Burakov, K., 1995. Archaeointensity of the geomagnetic field in the fifth
716 millennium B.C. in northern Mesopotamia. *Geomagn. Aeron.* 35, 398-402.
- 717 Nachasova, I., Burakov, K., 1998. Geomagnetic variations in the VI-V millennia B.C.
718 *Geomagn. Aeron.* 38, 502-505.
- 719 Nieuwenhuyse, O., Akkermans, P., van der Plicht, J., 2010. Not so coarse, nor always plain
720 -the earliest pottery of Syria. *Antiquity* 84, 71-85.
- 721 Nieuwenhuyse, O.P., Bernbeck, R., Akkermans, P.M.M.G., Rogasch, J., 2013. Interpreting
722 the Late Neolithic of Upper Mesopotamia, *Publications on Archaeology of the*
723 *Leiden Museum of Archaeology (PALMA)*, Brepols pub. (Turnhout, Belgium), 520
724 pp.

- 725 Nilsson, A., Snowball, I., Muscheler, R., Uvo, C.B., 2010. Holocene geocentric dipole tilt
726 model constrained by sedimentary paleomagnetic data. *Geochem. Geophys.*
727 *Geosyst.* 11, Q08018.
- 728 Nilsson, A., Holme, R., Korte, M., Suttie, N., Hill, M., 2014. Reconstructing Holocene
729 geomagnetic field variation: New methods, models and implications, *Geophys. J.*
730 *Int.* in press.
- 731 Nishiaki, Y., Le Mière, M., 2005. The oldest pottery Neolithic of Upper Mesopotamia: New
732 evidence from Tell Seker al-Aheimar, the Khabur, northeast Syria. *Paléorient* 31,
733 55-68.
- 734 Pavón-Carrasco, F.J., Osete, M.L., Torta, J.M., De Santis, A., 2014. A geomagnetic field
735 model for the Holocene based on archaeomagnetic and lava flow data. *Earth*
736 *Planet. Sci. Lett.* 388, 98-109.
- 737 Robert, B., Blanc, C., Chapoulie, R., Masetti-Rouault, M.-G., 2008. Characterizing the Halaf-
738 Ubaid Transitional Period by Studying Ceramic from Tell Masafkh, Syria.
739 *Archaeological Data and Archaeometry Investigations.* In : H. Kühne, R.M. Czichon,
740 F.J. Kreppner (eds.), *Social and Cultural Transformation : The Archaeology of the*
741 *Transitional Periods and Dark Ages Excavation Reports (Vol. 2), Proceedings of the*
742 *4th International Congress of Archaeology of the Near East, 29 March - 3 April*
743 *April 2004, Freie Universität Berlin, Harrassowitz Verlag, Wiesbaden, 225-234.*
- 744 Robert, B., 2009. Production céramique et représentations animales à l'époque de Halaf.
745 *Res Antiquae* 6, 271-292.
- 746 Robert, B., 2010. Développement et disparition de la production céramique halafienne:
747 implications techniques et sociales à partir d'études de cas. PhD thesis Université
748 Lumière Lyon 2, pp. 899.
- 749 Shaar, R., Ben-Yosef, E., Ron, H., Tauxe, L., Agnon, A., Kessel, R., 2011. Geomagnetic field
750 intensity: How high can it get? How fast can it change? Constraints from Iron-Age
751 copper-slag. *Earth Planet. Sci. Lett.* 301, 297-306.
- 752 Shaar, R., Tauxe, L., Ben-Yosef, E., Kassianidou, V., Lorentzen, B., Feinberg, J.M., Levy, T.E.,
753 2014. Decadal-scale variations in geomagnetic field intensity from ancient Cypriot
754 slag mounds. *Geochem. Geophys. Geosyst.* In press.

- 755 Tema, E., Kondopoulou, D., 2011. Secular variation of the Earth's magnetic field in the
756 Balkan region during the last eight millennia based on archaeomagnetic data.
757 *Geophys. J. Int.* 186(2), 603-614.
- 758 Thébault, E., Gallet, Y., 2010. A bootstrap algorithm for deriving the archeomagnetic field
759 intensity variation curve in the Middle East over the past 4 millennia BC. *Geophys.*
760 *Res. Lett.* 37, L22303. Doi:10.1029/2010GL044788.
- 761 Thellier, E., Thellier, O., 1959. Sur l'intensité du champ magnétique terrestre dans le
762 passé historique et géologique. *Ann. Géophys.* 15, 285-376
- 763 Tsuneki, A., Miyake, Y., 1996. The earliest pottery sequence of the Levant: New data from
764 Tell el-Kerkh 2, Northern Syria. *Paléorient* 22, 109-123.
- 765 Usoskin, I.G., Hulot, G., Gallet, Y., Roth, R., Licht, A., Joos, F., Kovaltsov, G.A., Thébault, E.,
766 Khokhlov, A., 2014. Evidence for distinct modes of solar activity. *Astronomy &*
767 *Astrophysics* 562, L10.
- 768 Valet J.-P., Herrero-Bervera, E. Le Mouél, J.-L., Plénier, G., 2008. Secular variation of the
769 geomagnetic dipole during the past 2000 years. *Geochem. Geophys. Geosyst.* 9,
770 Q01008.
- 771 Van der Plicht, J., Akkermans, P.M., Nieuwenhuyse, O.P., Kaneda, A., Russell, A.L., 2011.
772 Tell Sabi Abyad, Syria: radiocarbon chronology, cultural change, and the 8.2 ka
773 event. *Radiocarbon* 53(2), 229-243.
- 774 Yu, Y., Tauxe, L., Genevey, A., 2004. Toward an optimal geomagnetic field intensity
775 determination technique. *Geochem. Geophys. Geosyst.* 5(2), Q02H07.
- 776

777 **Table caption**

778 **Table 1.** Pottery group-mean intensity values obtained at Tell Halula ($\lambda=36^{\circ}25'N$,
 779 $\varphi=38^{\circ}10'E$; pottery groups SY127 to SY132) and Tell Masaikh ($\lambda=34^{\circ}25'N$, $\varphi=40^{\circ}01'E$;
 780 pottery groups SY37 and SY38). Information on the different archeological dating,
 781 relative chronology and references are provided in the second, third and fourth
 782 columns. See text for references on absolute dating (fifth column). * indicates that an
 783 approximation was made on the dating (see text). The mean intensity values and their
 784 standard deviations are provided in column 6. Column 7 shows the number Nb of
 785 fragments (/n specimens) retained for computing the pottery group-mean intensity
 786 values.

787

788 **Figure captions**

789 **Fig. 1.** (a) Location of the two Syrian archeological sites studied herein (Tell Halula and
 790 Tell Masaikh) and of three other sites discussed in the text (Tell Halaf, Yarim Tepe II and
 791 Tell Sotto). ©Google Earth. (b) General view of the Tell Halula archeological site. ©
 792 Universitat Autònoma de Barcelona (UAB)/SAPPO.

793 **Fig. 2.** Examples of pottery sherds discovered at Tell Halula. These fragments are dated
 794 to phases I, II and III of the pre-Halaf (photos 1-2, 3-4 and 5-6, respectively), to the
 795 proto-Halaf (photos 7-8), and to the Early, Middle and Late Halaf (photos 9, 10-11 and
 796 12-13, respectively). © Universitat Autònoma de Barcelona (UAB)/SAPPO.

797 **Fig. 3.** Triaxe intensity data obtained for two specimens from Tell Halula (SY89-08,
 798 SY140-06). (a,c) Thermal demagnetization data; (b,d) Triaxe measurement series; (e)
 799 Archeointensity results at the specimen level. See text and further explanations in Le
 800 Goff and Gallet (2004).

801 **Fig. 4.** (a) Normalized IRM acquisition curves obtained for one fragment from each time
 802 level. (b-c) Two examples of hysteresis loop. (d-g) Four examples of normalized
 803 thermomagnetic low-field susceptibility (heating and cooling) curves obtained from
 804 fragments collected at Tell Halula. These fragments are dated to the pre-Halaf (d,e),
 805 Middle Halaf (f) and to the Late Halaf (g). (h) Hysteresis ratios (M_{RS}/M_s vs. H_{CR}/H_C)
 806 obtained at Tell Mardikh/Ebla (grey color, Gallet et al., 2014), Tell Masaikh (blue

807 triangles) and Tell Halula (see color code on the figure according to the archeological
808 periods of the fragments).

809 **Fig. 5.** Intensity data obtained from eight different archeomagnetic pottery groups (a-e,
810 Tell Halula; f, Tell Masaikh). Each colored curve on each of these plots shows the
811 intensity data obtained for one specimen over the temperature range of analysis (for
812 further explanations, see in Le Goff and Gallet, 2004). Altogether, the results from 93
813 specimens are hence reported in this Figure.

814 **Fig. 6.** Archeomagnetic field intensity variations recovered from the new data obtained
815 at Tell Halula (blue circles) and Tell Masaikh (blue triangles). All results are converted in
816 Virtual Axial Dipole Moments. The chronological time scale is provided in the text (see
817 also in Table 1).

818 **Fig. 7.** Comparison between our new archeointensity data (in blue) and previous results
819 obtained (a) from Yarim Tepe II and Tell Sotto (green circles and triangles, respectively),
820 two multi-level archeological sites located in North Iraq (Nachasova and Burakov, 1995,
821 1998) and (b) from Bulgaria (in red; Kovacheva et al., 2014). As discussed in the text, the
822 dating of the Yarim Tepe II and Tell Sotto data was modified from the original papers.
823 The solid vs. open circles indicate the intensity values obtained from several vs. one
824 specimen(s).

825 **Fig. 8.** Regional averaged geomagnetic field intensity variation curve in the Middle East
826 over the past 9000 years. The data were selected inside a 1000 km-radius circle around
827 the location $\lambda=36^{\circ}49'N$, $\varphi=40^{\circ}02'E$ (archeological site of Tell Halaf). All data were
828 transformed into VADM. Two different approaches were successively considered to
829 compute the curve. (a) We used sliding windows of 200 years shifted every 10 years and
830 the bootstrap technique for taking into account the experimental and age uncertainties
831 on the available intensity data. 1000 curves were hence computed and are shown here
832 the mean (thick black line), the minimum and the maximum VADM values obtained for
833 the different time windows. The Syrian data are also reported (blue dots) together with
834 all other available archeointensity data (grey dots) satisfying minimum selection criteria
835 (Genevey et al., 2008). (b) We used an iteratively reweighted least-squares algorithm,
836 combined with a bootstrap, modified from that of Thébault and Gallet (2010). The

837 continuous black line shows the maximum of probability, and the light blue lines its 95%
838 fluctuation envelope. The 95% confidence interval is displayed by the red lines.

839 **Fig. 9.** Comparison between the geomagnetic field intensity (transformed into VADM)
840 variation curve in the Middle East, with averaging over sliding windows of 500 years
841 (black lines; see text), and previous dipole field moment reconstructions. The
842 comparison is made with (a) the VADM variation curve computed by Knudsen et al.
843 (2008) using temporal and geographic averaging (in red), (b) dipole moment
844 reconstructions derived from different time-varying global geomagnetic field modeling
845 (blue lines, modeling proposed by Pavón-Carrasco et al., 2014; orange and green lines,
846 the pfm9k.1b and pfm9k.1a modeling proposed by Nilsson et al., 2014).

847

Figure 1

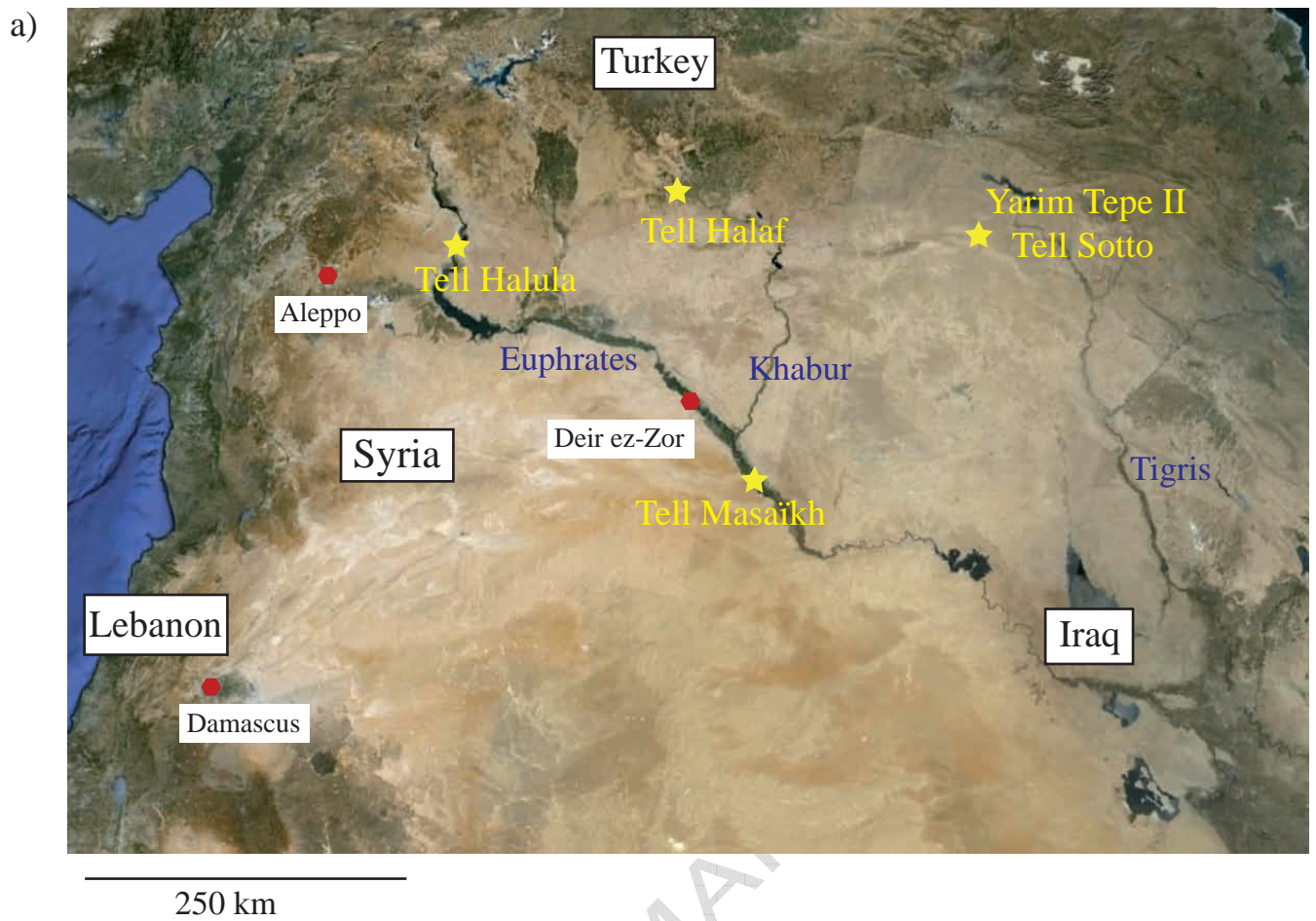


Figure 1

Figure 2



Figure 2

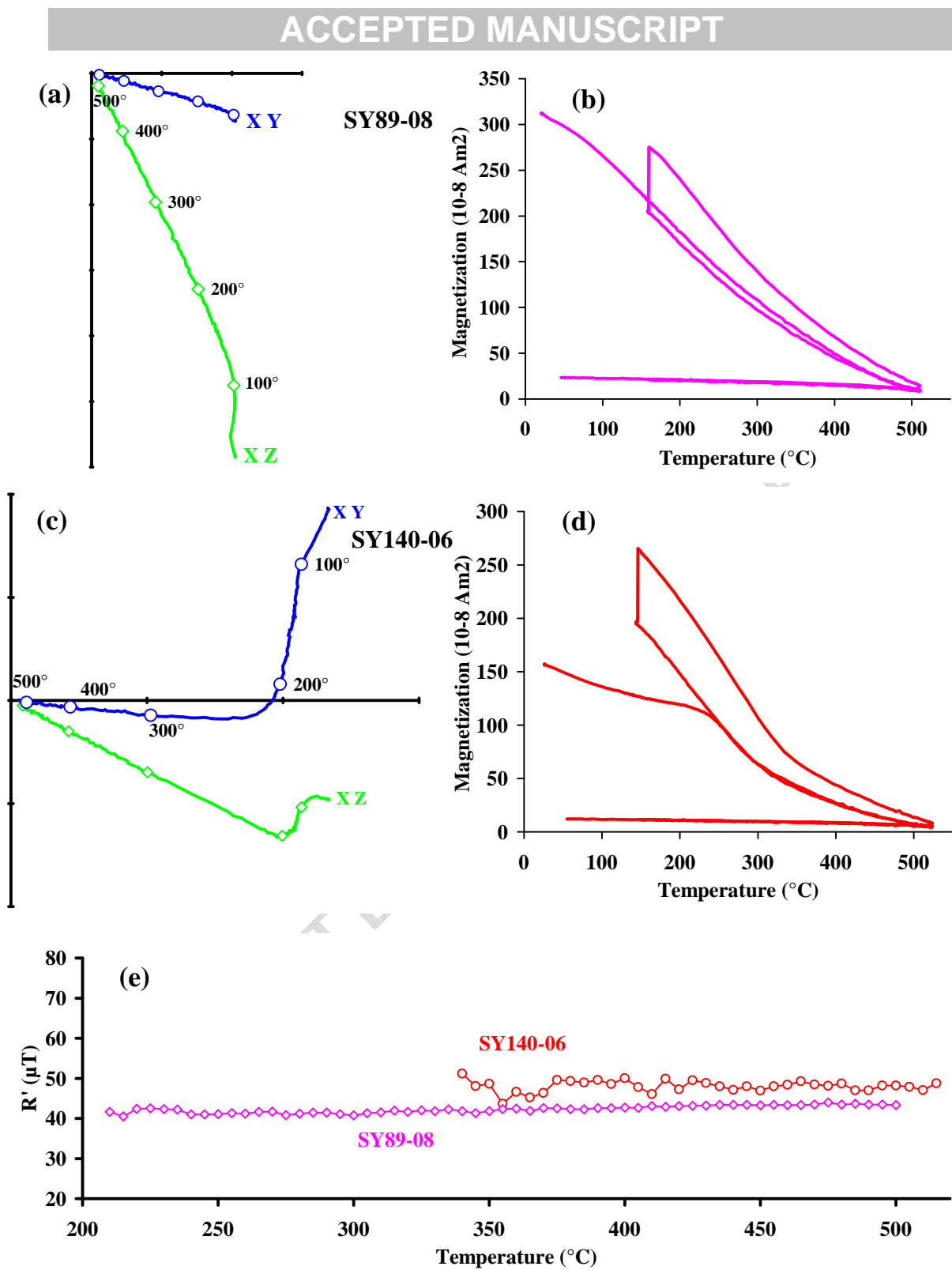


Figure 3

Figure 4

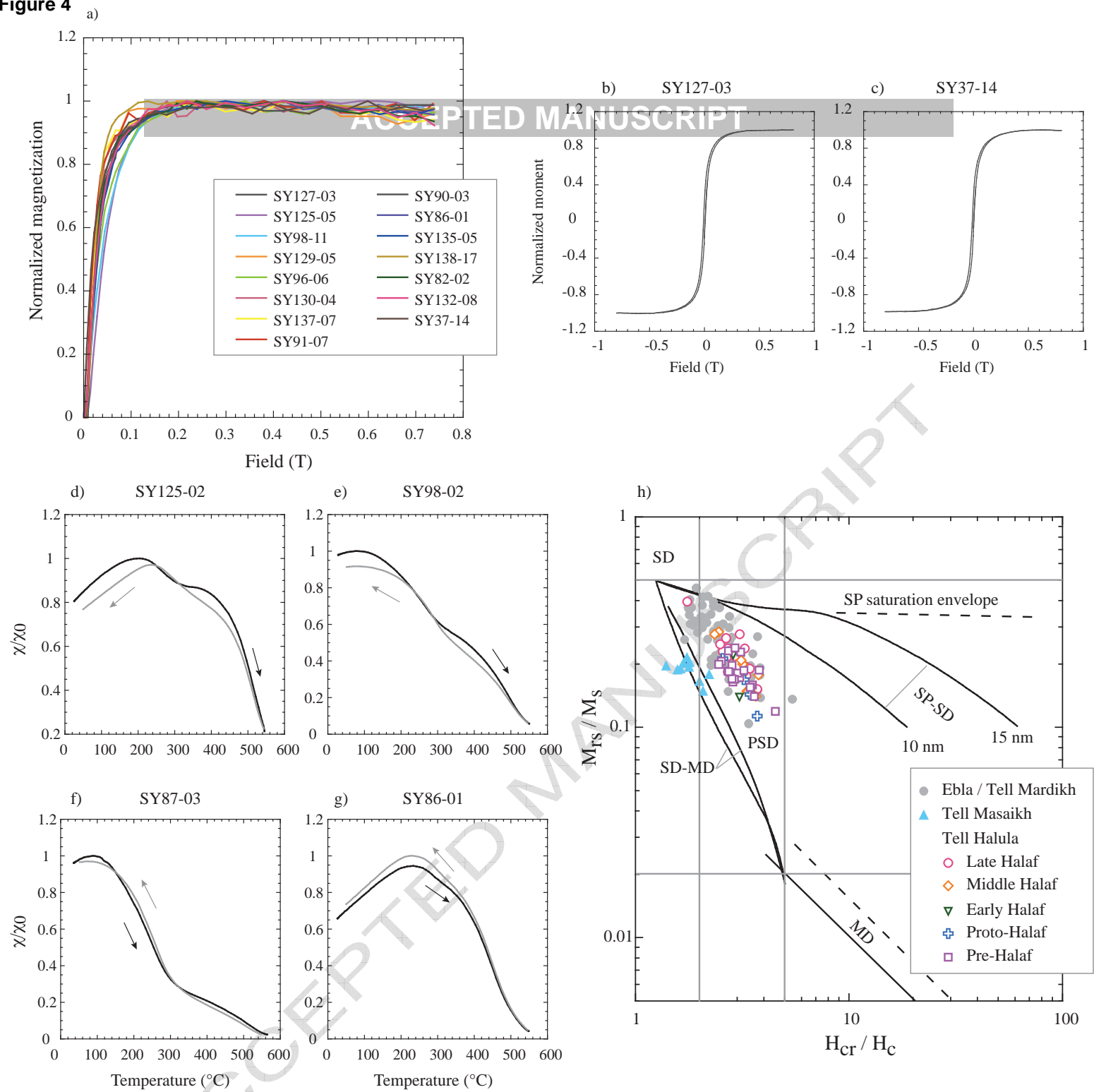


Figure 4

Figure 5

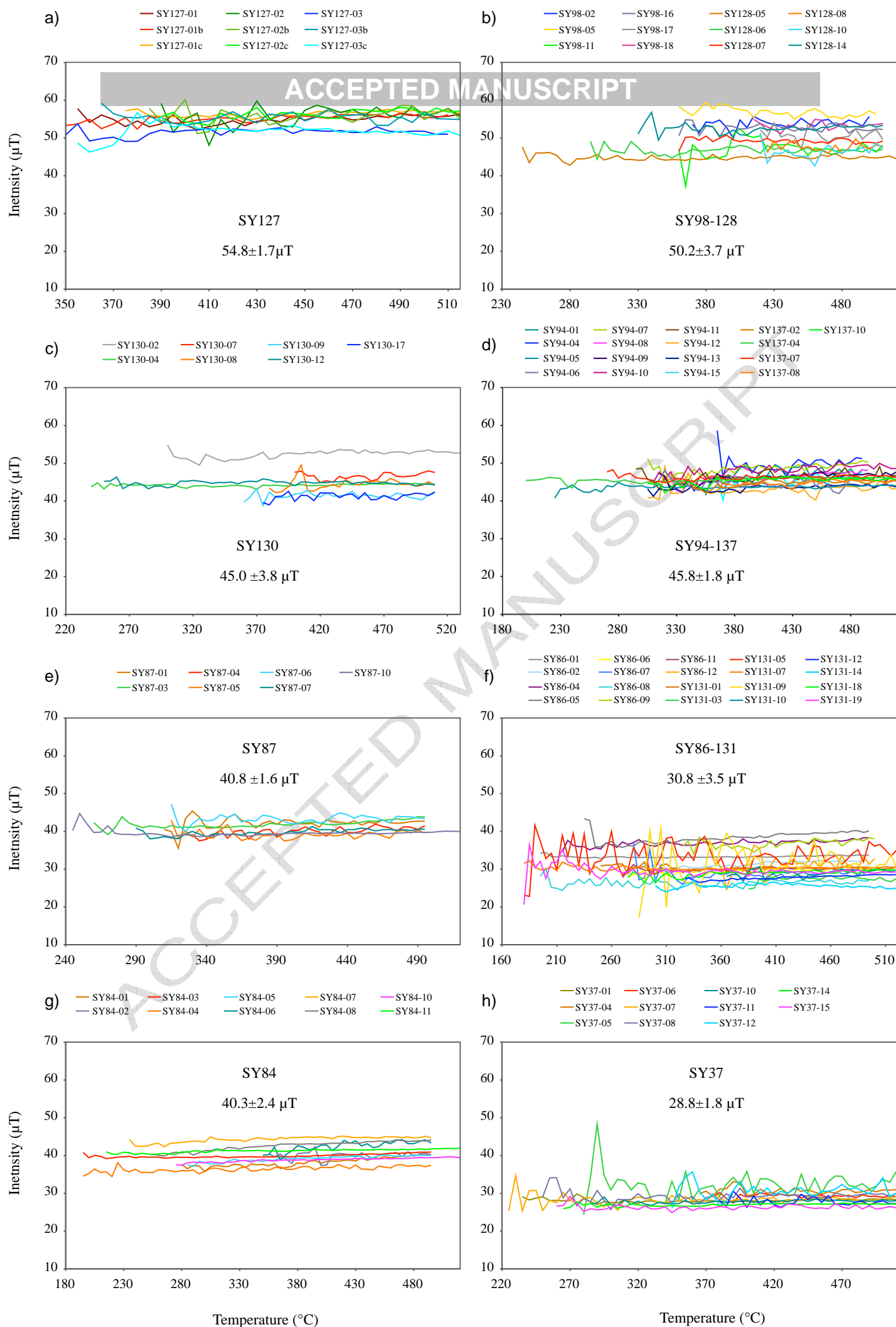


Figure 5

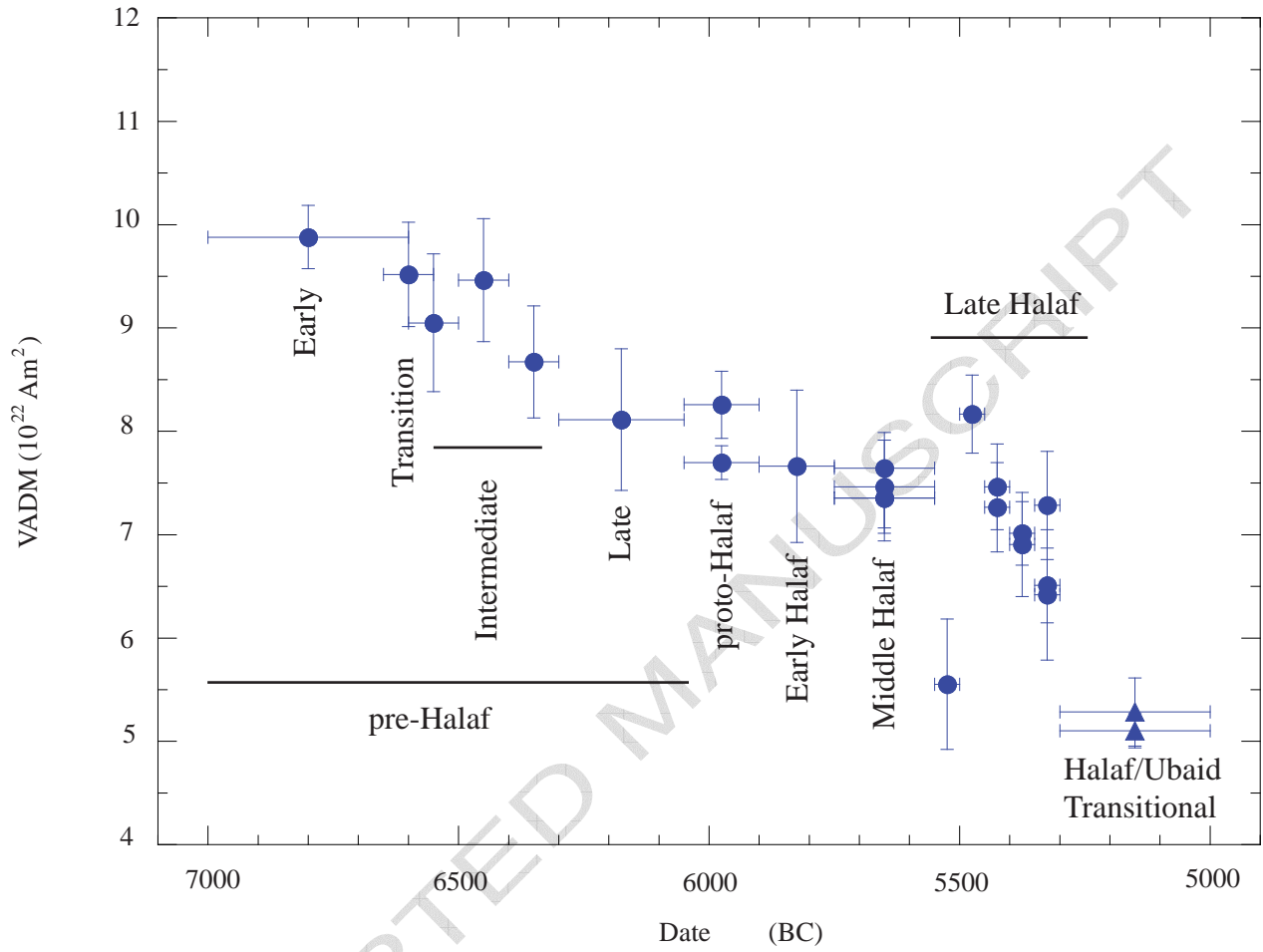


Figure 6

Figure 7

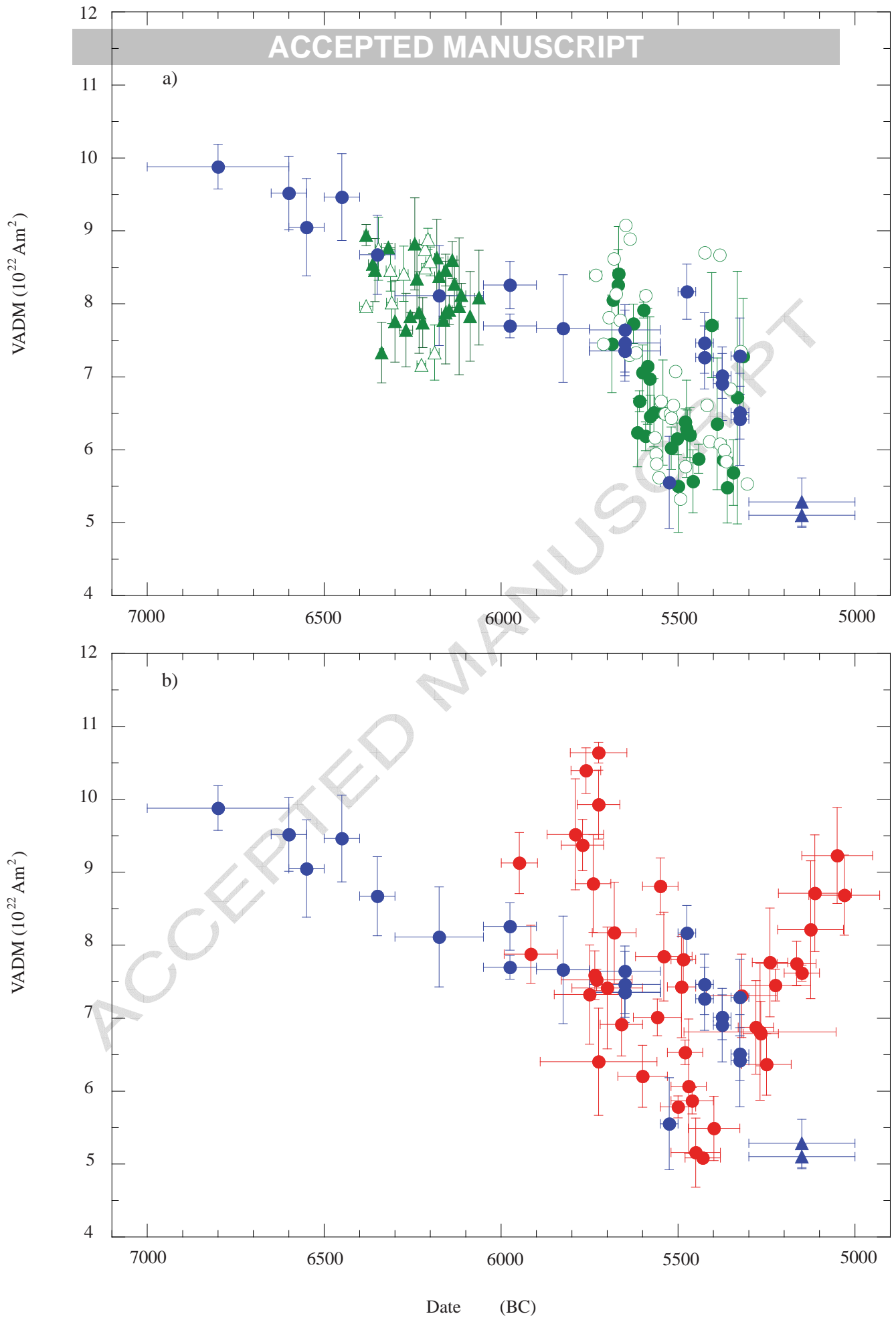


Figure 8

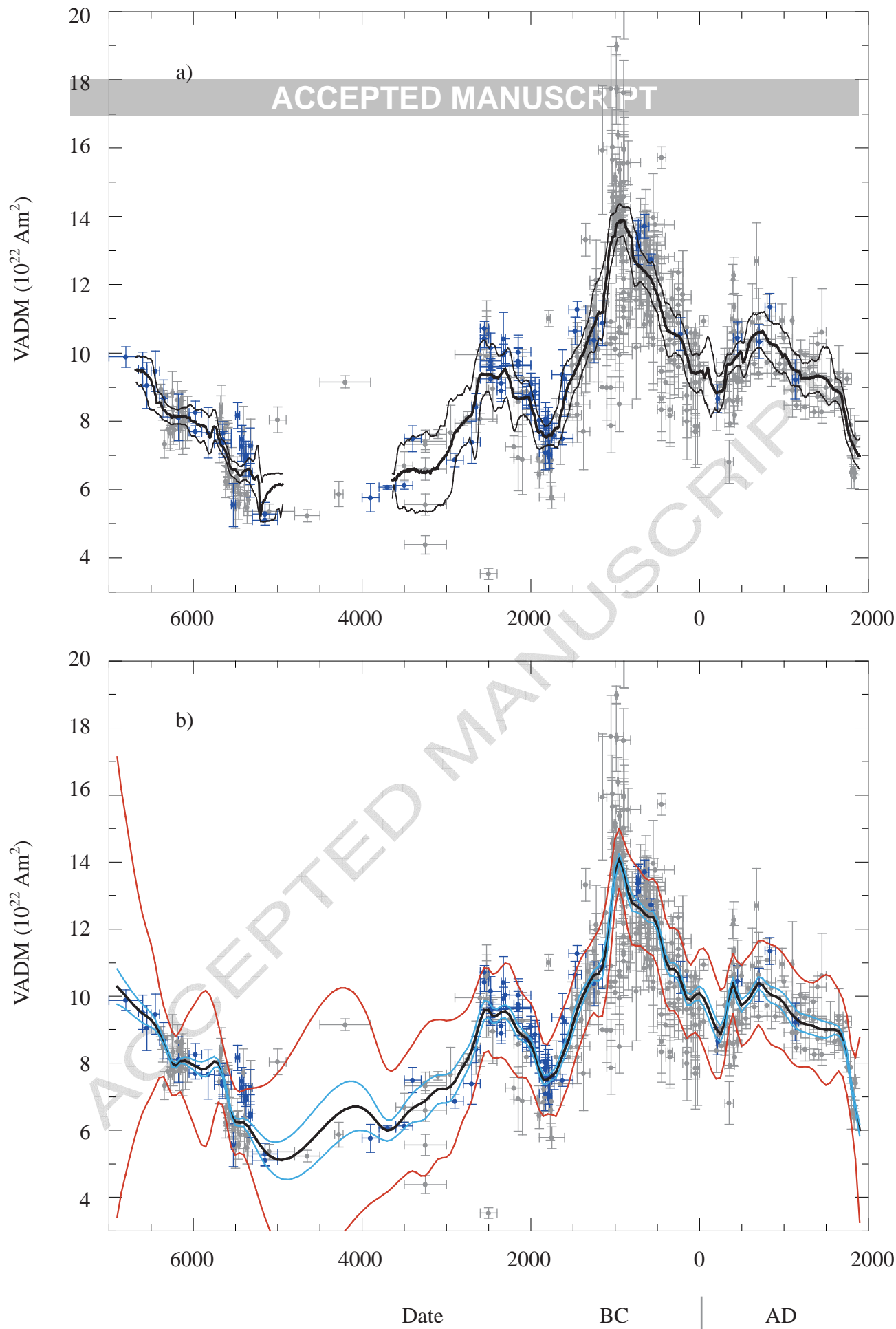


Figure 8

Figure 9

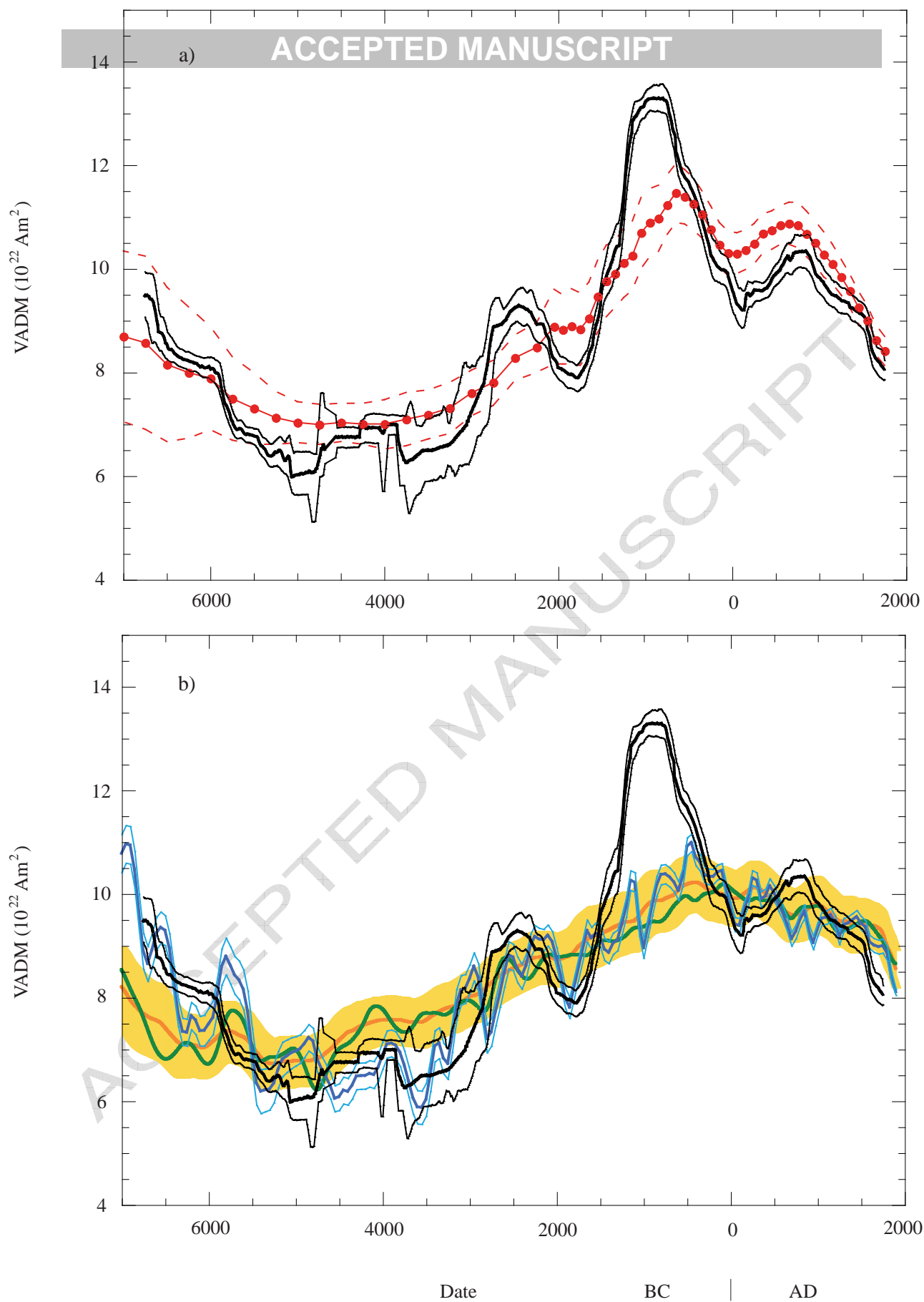


Figure 9

Pottery Group	Archeological Period	Relative chronology (Tell Halula)	Archeological reference	Age (BCE)	Intensity (μ T)	N frag. (n spec.)
ACCEPTED MANUSCRIPT						
SY127	Early Pre-Halaf	Phase I	Sector 2, square G, peat E1C	6800 \pm 200	54.8 \pm 1.7	3 (9)
SY125	Transition Early-Intermediate Pre-Halaf	Phase I/II	Sector 2, square I, A25	6600 \pm 50	52.8 \pm 2.8	2 (6)
SY98-128	Intermediate Pre-Halaf	Phase II -early phase	Sector SS14-Y, A6	6650 \pm 50*	50.2 \pm 3.7	12 (12)
SY97-129	Intermediate Pre-Halaf	Phase II -interm. Phase	Sector SS14-Y, A5a	6450 \pm 50*	52.5 \pm 3.3	17 (17)
SY96-140	Intermediate Pre-Halaf	Phase II -late phase	Sector SS14-Y, A3c	6350 \pm 50*	48.1 \pm 3.0	13 (13)
SY130	Late Pre-Halaf	Phase III	Sector 49, A9a, E25	6175 \pm 125	45.0 \pm 3.8	7 (7)
SY94-137	Proto-Halaf	Phase IV	Sector 44/3, A23, E27	5975 \pm 75	45.8 \pm 1.8	17 (17)
SY95	Proto-Halaf	Phase VI	Sector 40, A10	5975 \pm 75	42.7 \pm 0.9	5 (14)
SY91	Early Halaf	Phase V	Sector 44/4	5825 \pm 75	42.5 \pm 4.1	9 (9)
SY87	Middle Halaf	Phase VI	Sector 45, peat E5	5650 \pm 100	40.8 \pm 1.6	7 (7)
SY88	Middle Halaf	Phase VI	Sector 45, peat E9	5650 \pm 100	42.4 \pm 1.5	7 (7)
SY89	Middle Halaf	Phase VI	Sector 45, peat E1	5650 \pm 100	40.8 \pm 1.9	8 (8)
SY90	Middle Halaf	Phase VI	Sector 45, peat E3	5650 \pm 100	41.4 \pm 2.9	8 (8)
SY86-131	Late Halaf	Phase VII -early phase	Sector 49, A5	5525 \pm 25*	30.8 \pm 3.5	20 (20)
SY135	Late Halaf	Phase VII -interm./early Phase	Sector 49, A1g	5475 \pm 25*	45.3 \pm 2.1	11 (11)
SY84	Late Halaf	Phase VII -interm./interm Phase	Sector 49, A1c	5425 \pm 25*	40.3 \pm 2.4	10 (10)
SY138	Late Halaf	Phase VII -interm./interm. Phase	Sector 49, A1c, E8	5425 \pm 25*	41.4 \pm 2.3	11 (11)
SY82	Late Halaf	Phase VII -interm./late Phase	Sector 49, A7	5375 \pm 25*	38.3 \pm 2.8	7 (7)
SY83-136	Late Halaf	Phase VII -interm./late phase	Sector 49, A1b	5375 \pm 25*	38.9 \pm 1.7	13 (13)
SY80	Late Halaf	Phase VII -late phase	Sector 49, A7d, peat 24	5325 \pm 25*	35.6 \pm 3.5	8 (8)
SY81	Late Halaf	Phase VII -late phase	Sector 49, A7c, peat 32	5325 \pm 25*	36.1 \pm 2.0	6 (6)
SY132	Late Halaf	Phase VII -late phase	Sector 49, A7a, E21	5325 \pm 25*	40.4 \pm 2.9	8 (8)
SY37	Halaf-Ubaid Transitional	-	Locus K171 I/2, layer E2	5150 \pm 150	28.8 \pm 1.8	11 (11)
SY38	Halaf-Ubaid Transitional	-	Locus K171 I, floor E7	5150 \pm 150	27.8 \pm 0.9	5 (15)

Table 1

848 New archeomagnetic intensity data from two Syrian Late Neolithic archeological sites
849
850 We recover the regional geomagnetic intensity variations between ~7000 BC and
851 ~5000 BC
852
853 A 9000-years long archeointensity variation curve is constructed for the Middle East
854
855 We constrain the variations in the dipole field moment over most of the Holocene
856
857

ACCEPTED MANUSCRIPT